Understanding Small-Signal Grid Strength and Its Implication on Sub-/Supersynchronous Stability Risks

Yonggang Zhang*, Abdalrhman Hamad Fakhouri, Hongyu Jin
Department of Sustainable Electrical Energy Systems, 34121 Kassel, Germany
*E-mail: yonggang.zhang@uni-kassel.de

***Abstract*—Aiming to characterize the capacity ratio of the future GFM-converter dominated grid and massive GFL power infeeds under non-saturation conditions, the definitions of several SCR-based grid strength metrics are revisited and extended from the perspective of small-signal circuit ratio. Complex-valued grid-strength indicators are utilised to incorporate full RLC effects. The relation of node-specific ESCR and system-level gSCR is established. Their advantages and limitations in predicting the sub-/supersynchronous stability risks of GFL converters are revealed. Combining the participation factors of gSCR with the (individual) critical SCRs (CSCRs) of heterogeneous GFL devices, a method for estimating the system-level critical gSCR (i.e. CgSCR*) is proposed, facilitating the stability risk screening without the need of running complex small-signal analysis or time-consuming EMT simulations. Theoretical analysis results are validated by EMT simulations.**

***Index Terms*—Grid strength, CSCR, ESCR, gSCR, SSO.**

I. Introduction

The stability of modern power systems is challenged by the large-scale integration of heterogeneous grid-following (GFL) converters. One particular issue is the small-signal synchronisation instability of GFL devices that tends to be induced by weak grid strength, as usually quantified by short-circuit ratio (SCR) [1]. For a GFL converter, the existence of phase lock loop (PLL) intrinsically induces negative resistance within the PLL bandwidth around fundamental frequency f_1, and the existence of current control loop shapes the GFL impedance as capacitive in the $1.1f_1$-$2f_1$ frequency range, which together inevitably induces the sub-/supersynchronous oscillation (SSO) risk, given a sufficiently small SCR for a typical inductive grid connection [2]. For a single machine (GFL) infinite bus (SMIB) system, the required minimum or critical SCR (CSCR) for maintaining GFL stability depends on its control and operating condition, e.g. voltage deviation [3]. Such impacts on CSCR can be found in [2], [4]. Note that CSCR can be obtained either by EMT-simulation or small-signal analysis. Knowing CSCR of the GFL device and SCR of the grid, the stability risk can be predicted by checking whether SCR>CSCR and how big the difference is [5], [6].

In traditional synchronous machine (SM) dominated grids without multiple GFL infeeds in proximity, the SCR metric can accurately capture the grid strength for both normal and fault conditions. However, as SMs are gradually replaced by GFL devices, which in turn requires the installation of grid-forming (GFM) devices for strengthening the grid, the SCR can no longer unify the grid strength definitions for normal and fault operating conditions, taking into account the saturated GFM behaviors [7]. In this background, large-signal strengths based on short-circuit calculations can be too conservative to be taken as small-signal strengths due to saturation. Having small-signal stability as the focus of the work, SCR-related metrics are only considered in small-signal sense for further analysis. To account for the effects of multiple GFL infeeds and their electrical proximity, the two metrics ESCR [8] and gSCR [5] are introduced, which well capture the node-specific and system-level strengths respectively. In contrast, aggregated metrics like composite or weighted SCRs are simpler but not accurate enough [8].

As SCR-based metrics only capture the network impedance feature in a relatively narrow frequency band (e.g. by evaluating passive impedances at f_1, flux and/or voltage control impedances at the subtransient timescale), frequency-dependent metrics are proposed such as the grid strength impedance metric (GSIM) [9] and impedance margin ratio (IMR) [7]. These metrics consider system wideband dynamics either excluding one device (by looking into the system from the device's view) or in a complete closed-loop form, providing profound insights into potential stability issues. Nevertheless, their reliance on detailed device-level control dynamics and the resulting high computational complexity can be a barrier for a quick grid strength assessment and early-stage stability risk screening. To achieve a balance between simplicity and frequency-dependency, a frequency-averaged grid impedance (FAGI) metric is proposed in [10], which however may not well retain accuracy of the impedance in relevant frequency ranges.

To retain simplicity and accuracy in a single grid strength metric and realize a fast SSO risk screening based on the CSCRs of heterogeneous GFL infeeds, this paper revisits and extends several typical SCR-based metrics, achieving the following contributions:

1) Definitions of SCR, ESCR and gSCR are unified and extended to include overall grid RLC effects, stressing the need of including resistive and capacitive effects (e.g. from loads and lines) in grid strength assessment.
2) Node-specific ESCR and system-level gSCR are related to each other, and their limitations in predicting the SSO risks of heterogeneous GFL systems are demonstrated.

This work was supported in part by the German Research Foundation (DFG) within the project "InterAcDC" (517518989), and in part by the German Ministry for Economic Affairs and Energy and the Projektraeger Juelich (PtJ) within the project "SysStab2030" (FKZ 03EI6122J).

979-8-3315-8138-1

3) Based on the CSCRs of heterogeneous GFL devices and their participation factors (PFs) to gSCR, a simple critical gSCR estimation method is proposed, greatly simplifying the system-level SSO risk screening.

II. Revisiting SCR-Based Grid Strength Metrics From A Small-Signal Perspective

Fig. 1 presents an illustrative test system. GFL devices are represented as Norton equivalents connected to buses $\{1\ldots n\}$, while GFM devices are represented as ideal voltage sources $\boldsymbol{u}_{\mathrm{N}}(s)$ (assuming $\Delta\boldsymbol{u}_{\mathrm{N}}(s)=0$) behind their input impedances that are absorbed into the AC network admittance matrix $\boldsymbol{Y}_{\mathrm{N}}(s)$. Internal buses of the AC network are eliminated by Kron-reduction. Frequency-coupling effect in the AC network is expected to appear in the power synchronisation frequency band, i.e. within $0.95f_1$-$1.05f_1$, thus is negligible for the grid strength evaluation and the SSO risks lying within 0-$0.95f_1$ and $1.05f_1$-$2f_1$ [2]. Taking the GFL current infeeds $\Delta\boldsymbol{i}_{\mathrm{K}}(s)$ as input and the node voltage responses $\Delta\boldsymbol{u}_{\mathrm{K}}(s)$ as output, close-loop transfer function (CLTF) of the system can be derived applying the Kirchhoff's voltage and current laws, as represented by

$$\Delta\boldsymbol{u}_{\mathrm{K}}(s)=(\boldsymbol{Y}_{\mathrm{N}}(s)+\boldsymbol{Y}_{\mathrm{A}}(s))^{-1}\Delta\boldsymbol{i}_{\mathrm{K}}(s)=\boldsymbol{Y}_{\mathrm{KK}}(s)^{-1}\Delta\boldsymbol{i}_{\mathrm{K}}(s)\,. \quad (1)$$

Note that the system description in (1) can be easily adapted to include the frequency coupling effects in GFL converters [6], [11], which is for easier illustration not detailed here.

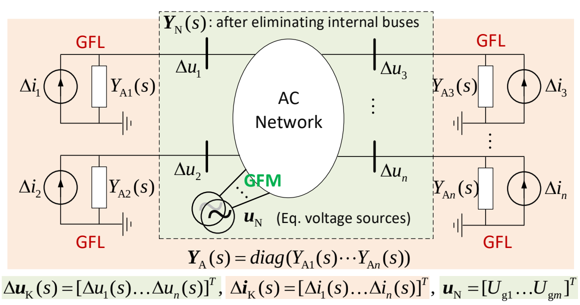

Fig. 1 An illustrative power system.

Assuming all GFL devices as ideal current sources, the equation (1) becomes

$$\Delta\boldsymbol{u}_{\mathrm{K}}(s)=\boldsymbol{Y}_{\mathrm{N}}(s)^{-1}\Delta\boldsymbol{i}_{\mathrm{K}}(s)=\boldsymbol{Y}_{\mathrm{N}}'(s)^{-1}\Delta\boldsymbol{i}_{\mathrm{K}}'(s) \quad (2)$$

where $\Delta\boldsymbol{i}_{\mathrm{K}}'(s)=\boldsymbol{S}_{\mathrm{A}}^{-1}\Delta\boldsymbol{i}_{\mathrm{K}}(s)$ is the multi-infeed current vector normalised by the device capacities $\boldsymbol{S}_{\mathrm{A}}=diag(S_{\mathrm{A1}}\ldots S_{\mathrm{A}n})$, resulting $\boldsymbol{Y}_{\mathrm{N}}'(s)=\boldsymbol{S}_{\mathrm{A}}^{-1}\boldsymbol{Y}_{\mathrm{N}}(s)$. All quantities are given in per unit on the base of S_{base} and U_{base}.

Neglecting all the GFL devices other than the one at the i-th node and assuming that it is operated at its rated power, the SCR at the i-th node can be evaluated as

$$SCR_i=\frac{S_{\mathrm{N}i}}{S_{\mathrm{A}i}}=\frac{U_{\mathrm{N}i}^{\ 2}}{S_{\mathrm{A}i}Z_{\mathrm{N}i}}=\frac{1}{S_{\mathrm{A}i}Z_{\mathrm{N}i}}=\frac{Y_{\mathrm{N}i}}{S_{\mathrm{A}i}}=\frac{\Delta i_i}{S_{\mathrm{A}i}\Delta u_i}=\frac{\Delta i_i'}{\Delta u_i}=Y_{\mathrm{N}i}' \quad (3)$$

where $S_{\mathrm{N}i}$ denotes the grid side small-signal power transfer capacity, $U_{\mathrm{N}i}=1$ is the nominal voltage in pu and $Z_{\mathrm{N}i}=X_{\mathrm{N}i}^{L}$ is assumed, resulting the SCR as a positive real value. Note that the quantities in (3) are at f_1, as indicated by removing the symbol s. For a generalized definition and the convenience of small-signal analysis, the network capacity $S_{\mathrm{N}i}$ and impedance $Z_{\mathrm{N}i}$ can be evaluated as complex values, taking into account the overall grid RLC effects at f_1, resulting in a complex-valued SCR. In SSO frequency ranges, particularly within $0.5f_1$-$0.9f_1$ or $1.1f_1$-$1.5f_1$ (where SSO often appear), the frequency-dependent admittance can be approximated to be

$$Y_{\mathrm{N}i}'(s)=\mathrm{Re}(SCR_i)+\mathrm{Im}(SCR_i)s/\omega_1=SCR_i(s)\,. \quad (4)$$

Note that the imaginary parts of the admittances in (3) and (4) that are contributed by GFM devices are extracted from their subtransient reactances corresponding to the frequencies of around $f_1\pm0.2f_1$, which are almost exclusively shaped by the voltage response dynamics for GFM devices (typically featured with the timescale of tens of milliseconds). In contrast, the synchronous reactances of GFM devices are more dominantly shaped by the power-frequency dynamics than by the voltage dynamics [2], thus are unable to reveal the voltage strength features. Analytically, after excluding the power-frequency dynamics of GFM devices, the remaining effects related to voltage strengths can be docomposed into: passive circuits and/or flux dynamics, AC voltage control (AVC), $Q(U)$-droop control, virtual impedances, etc. [2], [4]. Such decomposed impedance-shaping effects can then be evaluated at f_1.

Taking the GFM control without inner voltage loop in [2] as example, the subtransient impedance can be approximated as the sum of the virtual reactance X_{v} and the passive impedance R_{p}+jX_{p} at f_1. Similarly, $Q(U)$-droop can be equivalent to a virtual reactance and added in impedance [12]. Moreover, the AVC of SM can be equivalent to a virtual reactance based on the work in [4], while the GFM converter with voltage PI control can be approximated to be an ideal voltage source at the location where voltage is measured and controlled [12], [13]. Finally, the control effects of GFM devices can be integrated into the network admittance matrix $\boldsymbol{Y}_{\mathrm{N}}$, affecting the SCR-related indicators. Note that the virtual impedance and voltage PI control can largely change the SSO resistance for GFM [12], which requires careful treatment and further research.

Using the SCR metric defined in (3), the obtained voltage strength at the i-th node has not considered the effects of the neighboring GFL devices yet. One solution for this is to decouple the original MIMO system in (2) into multiple SISO systems as evaluated at f_1, as follows

$$\Delta\boldsymbol{i}_{\mathrm{K}}'=\underbrace{\boldsymbol{T}\Lambda_{\mathrm{N}}^{Y}\boldsymbol{L}}_{\boldsymbol{Y}_{\mathrm{N}}'}\Delta\boldsymbol{u}_{\mathrm{K}}\Leftrightarrow\underbrace{\boldsymbol{L}\Delta\boldsymbol{i}_{\mathrm{K}}'}_{\Delta\boldsymbol{i}_{\mathrm{T}}'}=\underbrace{diag(\Lambda_{\mathrm{N1}}^{Y}\ldots\Lambda_{\mathrm{N}n}^{Y})}_{\Lambda_{\mathrm{N}}^{Y}}\underbrace{\boldsymbol{L}\Delta\boldsymbol{u}_{K}}_{\Delta\boldsymbol{u}_{\mathrm{T}}} \quad (5)$$

where $\boldsymbol{L}=[\boldsymbol{l}_1\ \boldsymbol{l}_2\ \cdots\ \boldsymbol{l}_n]$ and $\boldsymbol{T}=[\boldsymbol{t}_1\ \boldsymbol{t}_2\ \cdots\ \boldsymbol{t}_n]$ are the left and right eigenvector matrices of the normalized $\boldsymbol{Y}_{\mathrm{N}}'$, respectively, satisfying $\boldsymbol{L}=\boldsymbol{T}^{-1}$ and $\boldsymbol{Y}_{\mathrm{N}}'\boldsymbol{T}=\boldsymbol{T}\Lambda_{\mathrm{N}}^{Y}$, with $\boldsymbol{l}_x=[l_{x1}\ l_{x2}\ \cdots\ l_{xn}]$ and $\boldsymbol{t}_x=[t_{1x}\ t_{2x}\ \cdots\ t_{nx}]^{\mathrm{T}}$ denoting the left-row and right-column eigenvectors of $\Lambda_{\mathrm{N}x}^{Y}$, respectively. Then $gSCR$ can be defined as the system-level weakest strength [5] relating $\Delta u_{\mathrm{T}x}=\Delta\boldsymbol{u}_{\mathrm{T}}(x)=\boldsymbol{l}_x\Delta\boldsymbol{u}_{\mathrm{K}}$ to $\Delta i_{\mathrm{T}x}'=\Delta\boldsymbol{i}_{\mathrm{T}}(x)'=\boldsymbol{l}_x\Delta\boldsymbol{i}_{\mathrm{K}}'$:

$$gSCR=\Delta i_{\mathrm{T}x}'/\Delta u_{\mathrm{T}x}=\min(\Lambda_{\mathrm{N1}}^{Y}\ldots\Lambda_{\mathrm{N}n}^{Y})\,. \quad (6)$$

As $\boldsymbol{t}_x$ is also the right eigenvector of $\Lambda_{\mathrm{N}x}^{Y\ -1}$ for $\boldsymbol{Z}_{\mathrm{N}}'=(\boldsymbol{Y}_{\mathrm{N}}')^{-1}$, we have $\boldsymbol{Z}_{\mathrm{N}}'\boldsymbol{t}_x=\Lambda_{\mathrm{N}x}^{Y\ -1}\boldsymbol{t}_x$ and $\sum_{j=1}^{n}Z_{ij}S_{\mathrm{A}j}t_{jx}=\Lambda_{\mathrm{N}x}^{Y\ -1}t_{ix}$ (by picking out the i-th equation), resulting in gSCR as:

979-8-3315-8138-1

$$gSCR = \Lambda_{\mathrm{N}x}^{Y} = \frac{\Delta i_{\mathrm{T}x}{}'}{\Delta u_{\mathrm{T}x}} = \frac{1/Z_{ii}}{S_{\mathrm{A}i} + \sum_{j=1, j\neq i}^{n} (Z_{ij}/Z_{ii})(t_{jx}/t_{ix}) S_{\mathrm{A}j}} . \quad (7)$$

To get the node-specific grid strengths, the *ESCR* metric is proposed by CIGRE [8]. For the node *i*, only the *i*-th voltage response to the multi-current infeeds is considered, resulting in

$$\Delta u_{\mathrm{i}} = \boldsymbol{Z}_{\mathrm{N}}(i,1:n)\Delta \boldsymbol{i}_{\mathrm{K}}(s) = \boldsymbol{Z}_{\mathrm{N}}(i,1:n)\boldsymbol{S}_{\mathrm{A}}\Delta \boldsymbol{i}_{\mathrm{K}}{}' . \quad (8)$$

Assuming the normalised infeeds satisfy $\Delta i_j{}' = \Delta i_i{}'$, i.e. $\Delta i_j / S_{\mathrm{A}j} = \Delta i_i / S_{\mathrm{A}i}$ for $i, j = 1\ldots n$ and solving (8) based on the definition of SCR in (3), the ESCR at node *i* can be defined as

$$ESCR_i = \frac{S_{\mathrm{N}i}}{S_{\mathrm{A}i}} = \frac{\Delta i_i}{S_{\mathrm{A}i}\Delta u_i} = \frac{\Delta i_i{}'}{\Delta u_i} = \frac{1/Z_{ii}}{S_{\mathrm{A}i} + \sum_{j=1, j\neq i}^{n} IF_{ji} S_{\mathrm{A}j}} \quad (9)$$

where $IF_{ji} = Z_{ij}/Z_{ii}$ denotes the interaction factor between the node *i* and *j*, as can be equivalent to $IF_{ji} = \Delta u_j / \Delta u_i$ [8].

Further, to bridge the relation of *gSCR* and $ESCR_{\mathrm{i}}$, we rewrite the matrix decoupling process in (5) as

$$\Delta \boldsymbol{u}_{\mathrm{K}} = \boldsymbol{T}(\boldsymbol{\Lambda}_{\mathrm{N}}^{Y})^{-1}\boldsymbol{L}\Delta \boldsymbol{i}_{\mathrm{K}}{}' = \sum_{v=1}^{n} \frac{1}{\Lambda_{\mathrm{N}v}^{Y}} \underbrace{\boldsymbol{t}_v \boldsymbol{l}_v}_{\boldsymbol{P}_v} \Delta \boldsymbol{i}_{\mathrm{K}}{}' \approx \frac{1}{\Lambda_{\mathrm{N}x}^{Y}} \boldsymbol{P}_x \Delta \boldsymbol{i}_{\mathrm{K}}{}' \quad (10)$$

where $\Lambda_{\mathrm{N}x}^{Y}$ is the smallest grid eigen-admittance that could most possibly approximate the weakest system response, and $\boldsymbol{P}_x$ is the well-established PF matrix of $\Lambda_{\mathrm{N}x}^{Y}$ [14] with p_x^{ij} denoting its *(i,j)* entry. As PFs can relate eigen-quantities to nodal quantities, we try to correlate the eigen-admittances with the nodal admittances ($ESCR_{\mathrm{i}}$) using

$$\Lambda_{\mathrm{N}x}^{Y} \approx \sum\nolimits_{i=1}^{n} ESCR_i\, p_x^{ii} = \overline{ESCR}_x \quad (11)$$

where $\overline{ESCR}_x$ can be understood as the weighted *ESCR* for the eigen-admittance $\Lambda_{\mathrm{N}x}^{Y}$ (for *gSCR* as $\overline{ESCR}$), and p_x^{ii} denotes the *(i,i)* entry of $\boldsymbol{P}_x$. This relation is verified in section IV.

Lastly, the network eigen-admittances $\Lambda_{\mathrm{N}x}^{Y}$ in (5) including the gSCR in (6) and the node-specific $ESCR_{\mathrm{i}}$ in (9) could be extended to frequency-dependent admittances in the SSO frequency ranges applying the approximation in (4). For instance, the $\Lambda_{\mathrm{N}x}^{Y}$ evaluated at f_1 in (5) can be extended to

$$\Lambda_{\mathrm{N}x}^{Y}(s) = \mathrm{Re}(\Lambda_{\mathrm{N}x}^{Y}) + \mathrm{Im}(\Lambda_{\mathrm{N}x}^{Y}) s/\omega_1 . \quad (12)$$

III. Relation of SCR-Based Metrics and SSO Risks

The multi-infeed system in (1) is normalised with the GFL capacity matrix $\boldsymbol{S}_{\mathrm{A}}$ as

$$\Delta \boldsymbol{i}_{\mathrm{K}}{}'(s) = (\boldsymbol{Y}_{\mathrm{N}}{}'(s) + \boldsymbol{Y}_{\mathrm{A}}{}'(s))\Delta \boldsymbol{u}_{\mathrm{K}}(s) = \boldsymbol{Y}_{\mathrm{KK}}{}'(s)\Delta \boldsymbol{u}_{\mathrm{K}}(s) \quad (13)$$

where $\boldsymbol{Y}_{\mathrm{A}}{}'(s) = \boldsymbol{S}_{\mathrm{A}}{}^{-1}\boldsymbol{Y}_{\mathrm{A}}(s) = diag(Y_{\mathrm{A1}}{}'(s) \ldots Y_{\mathrm{A}n}{}'(s))$. Poles of the CLTF $\boldsymbol{G}(s) = (\boldsymbol{Y}_{\mathrm{KK}}{}'(s))^{-1}$ are equivalent to the roots of

$$\det(\boldsymbol{Y}_{\mathrm{KK}}{}'(s)) = \det(\boldsymbol{L}(s)\boldsymbol{Y}_{\mathrm{KK}}{}'(s)\boldsymbol{T}(s)) = \det(\boldsymbol{\Lambda}_{\mathrm{N}}^{Y}(s) + \boldsymbol{\Lambda}_{\mathrm{A}}^{Y}(s)) = 0 \quad (14)$$

where $\boldsymbol{L}$(s) and $\boldsymbol{T}$(s) denote the eigen-vector matrices decouping $\boldsymbol{Y}_{\mathrm{N}}{}'$(s), and *s* can be understood as j*ω* to ensure the validity of the expression at least for numerical evaluations. Then we approximate (14) by simplifying $\boldsymbol{L}$(s) and $\boldsymbol{T}$(s) to $\boldsymbol{L}$ and $\boldsymbol{T}$ as used in (5) for the SSO frequency ranges, resulting in the (*x*, *x*) entries of $\boldsymbol{\Lambda}_{\mathrm{N}}^{Y}$ and $\boldsymbol{\Lambda}_{\mathrm{A}}^{Y}$ as [15]:

$$\Lambda_{\mathrm{N}x}^{Y}(s) = \sum_{i=1}^{n}\left(p_x^{ii} Y_i(s) + \frac{1}{2}\sum_{j=1, j\neq i}^{n} (p_x^{ii} + p_x^{jj} - p_x^{ij} - p_x^{ji}) Y_{ij}(s) \right) \quad (15)$$

$$\Lambda_{\mathrm{A}x}^{Y}(s) = \sum_{i=1}^{n} p_x^{ii} Y_{\mathrm{A}i}{}'(s) \quad (16)$$

where $Y_i(s)$ and $Y_{ij}(s)$ denote grid side shunt and series admittances connected at node *i* and between node *i* and *j*, respectively. The resulted $\boldsymbol{\Lambda}_{\mathrm{N}}^{Y}(s)$ is diagonal, while the $\boldsymbol{\Lambda}_{\mathrm{A}}^{Y}(s)$ is only diagonal when all GFL devices are homogeneous, i.e. $\boldsymbol{Y}_{\mathrm{A}}{}'(s) = Y_{\mathrm{A}i}{}'(s)\boldsymbol{I}_n$ $(i = 1\ldots n)$ where $\boldsymbol{I}_{\mathrm{n}}$ is an identity matrix. This can be explained by $\boldsymbol{\Lambda}_{\mathrm{A}}^{Y}(s) = \boldsymbol{L}\boldsymbol{Y}_{\mathrm{A}}{}'(s)\boldsymbol{T} = \boldsymbol{Y}_{\mathrm{A}}{}'(s)$. In this special case, the roots of (14) are decoupled into

$$\prod_{x=1}^{n}(\Lambda_{\mathrm{N}x}^{Y}(s) + \Lambda_{\mathrm{A}x}^{Y}(s)) = \prod_{x=1}^{n}(\Lambda_{\mathrm{N}x}^{Y}(s) + Y_{\mathrm{A}i}{}'(s)) = 0 \quad (17)$$

for $i = 1\ldots n$. The MIMO system stability is thus decoupled into SISO system stabilities indicated by $\Lambda_{\mathrm{N}x}^{Y}(s) + Y_{\mathrm{A}i}{}'(s) = 0$.

Instead of evaluating the roots of (14) or (17) with detailed small-signal analysis, the SCR-based grid strength metrics provide an easier way for estimating the stability of SSO modes. Typically, given the CSCRs of individual GFL devices that can be derived using SMIB systems, there is a dominant root of $SCR(s) + Y_{\mathrm{A}}(s) = 0$ with zero damping (marginally stable) at *SCR*=*CSCR* for each GFL device. The damping of the mode (if the mode still exists) will become positive if *SCR*>*CSCR* (typically along with a larger mode frequency) and negative if *SCR*<*CSCR* (typically along with a smaller mode frequency), mainly because the PLL-induced negative resistance becomes larger as the mode frequency shifts towards f_1 in the supersynchronous frequency range [2], [5], [6].

For multi-infeed systems, similar analysis as above could be made using $ESCR_{\mathrm{i}}$ and $CSCR_{\mathrm{i}}$ for *i*=1…*n*, which however could not strictly consider the couplings among grid nodes. Since the smallest grid eigen-admittance gSCR indicates the weakest *virtual* node of the grid, the system stability can be most possibly constrained by the CgSCR, as indicated by the critical mode in $\Lambda_{\mathrm{N}x}^{Y}(s) + \Lambda_{\mathrm{A}x}^{Y}(s) = 0$ where $\Lambda_{\mathrm{N}x}^{Y}(s) = gSCR(s)$. However, the critical gSCR (CgSCR) for system stability is usually not known and it may depend on the CSCRs of multiple GFL devices. In this regard, we combine the PFs of gSCR and the CSCRs of GFLs to estimate the CgSCR, as formulated in

$$CgSCR^{*} = \sum\nolimits_{i=1}^{n} p_x^{ii} CSCR_i . \quad (18)$$

However, the system stability may not be exclusively determined by a single CgSCR. For instance, when there are two or more subsystems with (very) weak connection(s), the heterogeneous GFL devices in different subsystems may have their individual SSO risks that are mainly determined by the local grid strengths. In this case, the node-specific ESCR can be more useful than a single system-level gSCR. Alternatively, a group of small eigen-admittances from $\Lambda_{\mathrm{N1}}^{Y} \ldots \Lambda_{\mathrm{N}n}^{Y}$ (including *gSCR*) should be used for analysis, requiring the estimation of multile CgSCRs using the PFs of these eigen-admittances.

IV. CASE STUDY

Fig. 2 shows the test system. Details on the converter control are referred to [4]. Test scenarios and analysis results are summarized in TABLE I. The cases are defined by varying the SCRs of the grids (assuming two separate SMIB systems), opening/closing the breakers, or exchanging the locations of the GFL devices.

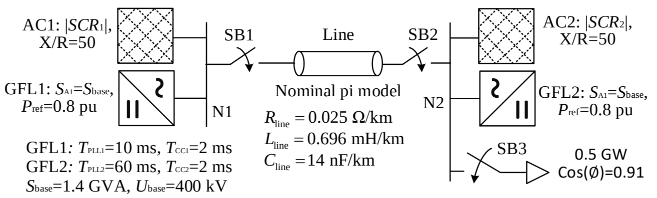

Fig. 2. A simple test grid with two subsystems.

In Case1, the breakers of the line (SB1 and SB2) and load (SB3) are opened. The *CSCR*s of GFL1 and GFL2 are obtained via EMT simulations for P_0=0.8 pu (by gradually reducing the SCRs of the two separated systems to reach marginally stable states). We also verify that for a random P>0, e.g. as 0.3, 0.5 or 0.9, the CSCRs can be well adapted for the adopted GFL devices applying $CSCR_i^{P} = CSCR_i^{P_0}\sqrt{P_0/P}$ [2]. On how voltage and reactive power Q can vary CSCR, some relevant results can be found such as in [16] but further research is still needed. For a fair comparison of all the cases in this work, Q=0 is used, and a similar voltage is maintained.

In Case2-Case4, the breakers of the line are closed. Case2 and Case3 show the stability of the system dominated either by GFL1 or by GFL2, and exchanging the locations of GFL1 and GFL2 show completely different stability results. In Case3, the large load resistive effect is demonstrated. In Case4, the long line capacitive effect is revealed.

Then we use Case2a to illustrate the composition of the grid eigen-admittances (the smallest one as gSCR) derived in (10), (15) and (17) in a symbolic way, as represented by

$$\begin{aligned} \Lambda_{\mathrm{N1}}^{Y} &= 0.91SCR_1 + 0.09SCR_2 + 0.44Y_{Line}^{RL} = 1.98\angle -87^{\circ} \\ \Lambda_{\mathrm{N2}}^{Y} &= 0.09SCR_1 + 0.91SCR_2 + 1.6Y_{Line}^{RL} = 7.4\angle -87^{\circ} \end{aligned} \tag{19}$$

where the small capacitive admittances of the line are omitted for stressing the main contributors, and the complex-valued PFs are simplified to their magnitudes. It is worth stressing that, even with large series admittances (toward zero impedances), the grid strengths are still constrained by the sum of the parallel admittances of the AC grids (AC1 and AC2). On this basis, the eigen-admittance $\Lambda_{\mathrm{N2}}^{Y} = 7.4\angle -87^{\circ}$ (with $1.6Y_{Line}^{RL} \approx 2.43$) exceeds the sum of $|SCR_1|$=1.0 and $|SCR_2|$=5.5, thus is not a reasonable grid strength indicator.

Accordingly, in Case2a, the heterogeneity of GFL devices results in a non-diagonal $\Lambda_{\mathrm{A}}^{Y}(s)$, as represented by

$$\Lambda_{\mathrm{A}}^{Y}(s) = \begin{bmatrix} 0.91Y_{\mathrm{A1}}'(s) + 0.09Y_{\mathrm{A2}}'(s) & -0.28Y_{\mathrm{A1}}'(s) + 0.28Y_{\mathrm{A2}}'(s) \\ -0.28Y_{\mathrm{A1}}'(s) + 0.28Y_{\mathrm{A2}}'(s) & 0.09Y_{\mathrm{A1}}'(s) + 0.91Y_{\mathrm{A2}}'(s) \end{bmatrix} \tag{20}$$

Therefore, the system stability still depends on $\det(\Lambda_{\mathrm{N}}^{Y}(s) + \Lambda_{\mathrm{A}}^{Y}(s)) = 0$ instead of $\prod_{x=1,2} (\Lambda_{\mathrm{N}x}^{Y}(s) + \Lambda_{\mathrm{A}x}^{Y}(s)) = 0$ according to (17). Neglecting the non-diagonal entries in $\Lambda_{\mathrm{A}}^{Y}(s)$ can inevitably introduce an error in stability judgement. Bearing such an error, system stability can be predicted by comparing gSCR with $CgSCR^{*}$ for the SISO system represented by $\Lambda_{\mathrm{N1}}^{Y}(s)$ and $\Lambda_{\mathrm{A1}}^{Y}(s) = 0.91Y_{\mathrm{A1}}'(s) + 0.09Y_{\mathrm{A2}}'(s)$. With this, another error is induced by estimating the *CgSCR*, unless the *CgSCR* is obtained by running detailed small-signal analysis or EMT simulation. Alternatively, the system stability can be more simply judged by comparing $ESCR_i$ with $CSCR_i$, which however further simplifies the coupling among grid nodes and thus introduces extra errors. Notably, the resistive effect of the transmission line (quantified by X/R=10, lying in the typical range of 5-20) also influences the SSO risk, as it varies the angle of SCR-based metrics. The theoretical analysis to Case2a aligns well with the numerical results in TABLE I.

In Case2b, the locations of GFL1 and GFL2 are exchanged in contrast to Case2a, without changing the *gSCR* (i.e. $\Lambda_{\mathrm{N1}}^{Y}$ as the smallest eigen-admittance applied to all cases) and *ESCRs*, but the $|CgSCR^{*}|$ is varied from 2.03 to 1.425, resulting an obvious relation of $|gSCR|>|CgSCR^{*}|$ and a stable system.

TABLE I. A summary of the test scenarios and results: × is "open" and ✓ is "close" for breaker(s), and the smallest eigen-admittance is gSCR.

	Node strengths	Eigen-strengths	PFs and other info	Extended indicators	EMT results
Case1: Line ×, Load × $CSCR_1$=SCR_1=**2.09**$\angle -89°$ $CSCR_2$=$SCR2$=**1.37**$\angle -89°$	$ESCR_1$=SCR_1 $ESCR_2$= SCR_2	$gSCR = \Lambda_{\mathrm{N1}}^{Y} = SCR_2$ $\Lambda_{\mathrm{N2}}^{Y} = SCR_1$	$\lvert p_1^{11}\rvert = 0$, $\lvert p_1^{22}\rvert = 1.0$ $\lvert p_2^{11}\rvert = 1.0$, $\lvert p_2^{22}\rvert = 0$	$\overline{ESCR} = SCR_2$ $CgSCR^{*} = SCR_2$	GFL1: ζ≈0 at **13** Hz GFL2: ζ≈0 at **4.5** Hz
Case2a: Line ✓, Load × $\lvert SCR_1\rvert$ = 1.0 $\lvert SCR_2\rvert$ = 5.5	$ESCR_1$=1.7$\angle -87°$ $ESCR_2$=3.7$\angle -89°$	$\Lambda_{\mathrm{N1}}^{Y} = \mathbf{1.98}\angle -87^{\circ}$ $\Lambda_{\mathrm{N2}}^{Y} = 7.4\angle -87^{\circ}$	$\lvert p_1^{11}\rvert = 0.91$, $\lvert p_1^{22}\rvert = 0.09$ $\Lambda_{\mathrm{N1}}^{Y} = \mathbf{2.05}\angle -87^{\circ}$ excl. C	$\overline{ESCR} = 1.9\angle -87^{\circ}$ $CgSCR^{*} = \mathbf{2.03}\angle -88^{\circ}$	GFL1: ζ≈0 at **12** Hz GFL2: ζ≈0 at **12** Hz
Case2b: GFL2 at N1, GFL1 at N2 in contrast to **Case2a**	*Same as* ***Case2a***	*Same as* ***Case2a***	*Same as* ***Case2a***	$\overline{ESCR} = 1.9\angle -87^{\circ}$ $CgSCR^{*} = \mathbf{1.425}\angle -88^{\circ}$	System **very stable**
Case3a: Line ✓, Load × $\lvert SCR_1\rvert$ = 3.5 $\lvert SCR_2\rvert$ = 0.5	$ESCR_1$=2.1$\angle -89°$ $ESCR_2$=1.1$\angle -87°$	$\Lambda_{\mathrm{N1}}^{Y} = \mathbf{1.31}\angle -87^{\circ}$ $\Lambda_{\mathrm{N2}}^{Y} = 5.6\angle -87^{\circ}$	$\lvert p_1^{11}\rvert = 0.15$, $\lvert p_1^{22}\rvert = 0.85$ $\Lambda_{\mathrm{N1}}^{Y} = \mathbf{1.38}\angle -87^{\circ}$ excl. C	$\overline{ESCR} = 1.27\angle -86^{\circ}$ $CgSCR^{*} = \mathbf{1.47}\angle -88^{\circ}$	GFL1: ζ≈0 at **4.8** Hz GFL2: ζ≈0 at **4.8** Hz
Case3b: GFL2 at N1, GFL1 at N2 in contrast to **Case3a**	*Same as* ***Case3a***	*Same as* ***Case3a***	*Same as* ***Case3a***	$\overline{ESCR} = 1.27\angle -86^{\circ}$ $CgSCR^{*} = \mathbf{1.98}\angle -88^{\circ}$	System **very unstable** with strong nonlinearity
Case3c: Line ✓, Load ✓ in contrast to **Case3a**	$ESCR_1$=2.3$\angle -83°$ $ESCR_2$=1.3$\angle -75°$	$\Lambda_{\mathrm{N1}}^{Y} = \mathbf{1.5}\angle \mathbf{-76^{o}}$ $\Lambda_{\mathrm{N2}}^{Y} = 5.6\angle -86^{\circ}$	$\lvert p_1^{11}\rvert = 0.16$, $\lvert p_1^{22}\rvert = 0.84$ $\Lambda_{\mathrm{N1}}^{Y} = \mathbf{2.1}\angle -90^{\circ}$ excl. $\boldsymbol{R}$	$\overline{ESCR} = 1.45\angle \mathbf{-73^{o}}$ $CgSCR^{*} = \mathbf{1.47}\angle -85^{\circ}$	**Well-damped 4** Hz mode
Case4a: Line ✓, Load × Line ↓ $\lvert SCR_1\rvert$ = 2.08 1500km, $\lvert SCR_2\rvert$ = 1.65	$ESCR_1$=1.63$\angle -89°$ $ESCR_2$=1.33$\angle -88°$	$\Lambda_{\mathrm{N1}}^{Y} = \mathbf{1.42}\angle -88^{\circ}$ $\Lambda_{\mathrm{N2}}^{Y} = 2.16\angle -87^{\circ}$	$\lvert p_1^{11}\rvert = 0.21$, $\lvert p_1^{22}\rvert = 0.79$ $\Lambda_{\mathrm{N1}}^{Y} = \mathbf{1.8}\angle -89^{\circ}$ excl. $\boldsymbol{C}$	$\overline{ESCR} = 1.4\angle -87^{\circ}$ $CgSCR^{*} = \mathbf{1.52}\angle -87^{\circ}$	GFL1: ζ≈0 at **11.5** Hz, **5** Hz observable GFL2: ζ≈0 at **5** Hz
Case4b: Line ✓, Load × Line↓(***C*=0)**, $\lvert SCR_1\rvert$ = 1.8 1500km, $\lvert SCR_2\rvert$ = 1.14	$ESCR_1$=1.69$\angle -89°$ $ESCR_2$=1.22$\angle -89°$	$\Lambda_{\mathrm{N1}}^{Y} = \mathbf{1.33}\angle -89^{\circ}$ $\Lambda_{\mathrm{N2}}^{Y} = 2.22\angle -89^{\circ}$	$\lvert p_1^{11}\rvert = 0.13$, $\lvert p_1^{22}\rvert = 0.87$	$\overline{ESCR} = 1.28\angle -88^{\circ}$ $CgSCR^{*} = \mathbf{1.46}\angle -88^{\circ}$	GFL1: ζ≈0 at **12** Hz, **4.5** Hz observable GFL2: ζ≈0 at **4.5** Hz

979-8-3315-8138-1

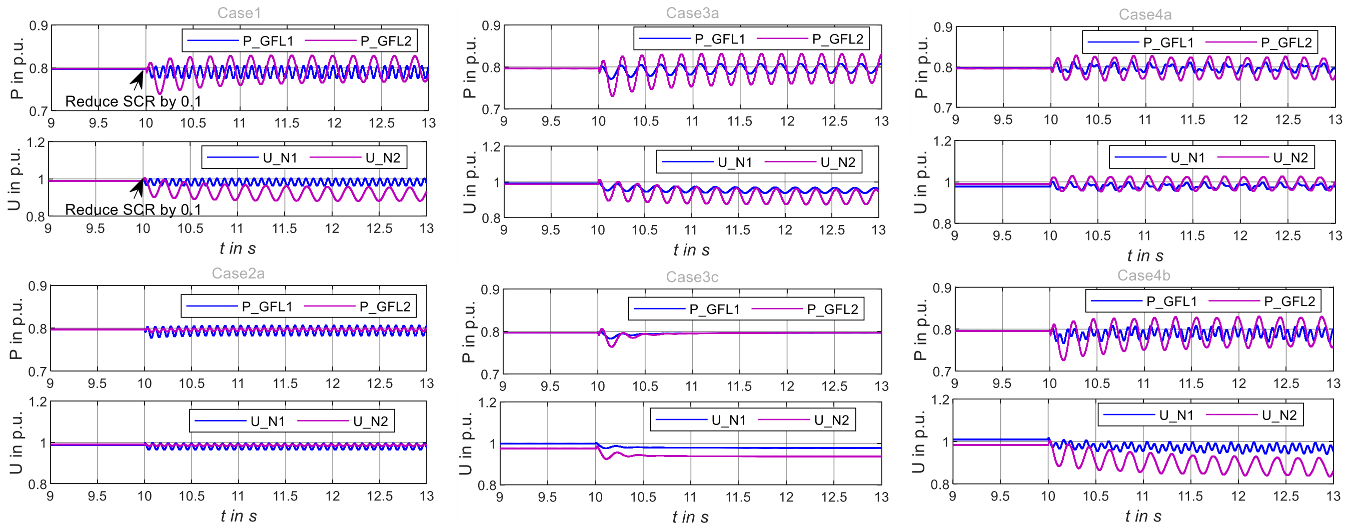

Fig. 3. EMT simulation results.

In Case3, a large SCR_1 and a small SCR_2 are adopted as compared to Case2, and the resistive effect from load is highlighted. As the result, the mode of GFL2 (4.5 Hz) can be excited. In Case3a, it is marginally stable considering the relation between *gSCR* and $CgSCR^*$ (including their angle difference) and the inevitable errors in stability prediction. In Case3b, it is very unstable due to an obvious relation of $|gSCR|<|CgSCR^*|$. In Case3c, it is very stable due to relation of $|gSCR|\approx|CgSCR^*|$ and the large load resistive effect. In Case4, the length of the line is increased from 300 km (1 pi section) to 1500 km (5 pi sections) to highlight the capacitive effect. In Case4b, by setting the C=0 and varying the SCR1 and SCR2 based on Case4a, it shows that, when there is no long line capacitive effect, the SSO risk can be noticeably changed.

V. Conclusion

This paper revisits and extends several SCR-based grid strength metrics from the perspective of small-signal circuit ratio (SSCR). Complex-valued grid admittances incorporating RLC effects are proven useful for assessing the GFL SSO risks under weak grid conditions. Node-specific ESCR is revealed as a multi-input single-output (MISO) indicator not fully accounting for grid admittance coupling between nodes, while the gSCR is shown to fully capture the grid side MIMO feature. Relation between ESCR and gSCR is built using the PFs of the gSCR. While gSCR can predict weak grid SSO risks for homogeneous GFL devices more accurately than ESCR, its accuracy decreases in cases of heterogeneous GFL devices, due to the simplification to the simultaneously mapped device admittance matrix when diagonalizing grid admittance matrix. To mitigate this impact, a method is proposed to estimate the CgSCR utilizing the individual CSCRs of GFL devices and the PFs of gSCR, which effectively captures the combined stability boundary determined by the grid and the heterogeneous GFL devices. Case studies validate the proposed approaches.

Future work could include verifying the proposed methods with bulk power systems, and assessing the system strength and SSO risks of hybrid AC/DC grids, taking into account the effects of different GFM control schemes and AC-DC coupling.

References

[1] X. Wang, M. G. Taul, H. Wu, Y. Liao, F. Blaabjerg, and L. Harnefors, "Grid-Synchronization Stability of Converter-Based Resources—An Overview," *IEEE Open J. Ind. Applicat.*, vol. 1, pp. 115–134, 2020.

[2] Y. Zhang, P. Unruh, B. Fischer, and M. Braun, "Comparative Impedance Characteristic Analysis of Grid‐Following and Grid‐Forming Inverters," *IET Renewable Power Generation*, vol. 19, no. 1, 2025.

[3] Z. Sui, Q. Sun, R. Wang, and P. Wang, "A New Method for Broadband Oscillation Analysis of the Grid-Following Converter," *IEEE Trans. Ind. Electron.*, pp. 1–13, 2025, doi: 10.1109/TIE.2025.3591647.

[4] Y. Zhang et al., "On the control interaction of synchronous machine and inverter-based resources during system-split situations," *International Journal of Electrical Power & Energy Systems*, vol. 152, 2023.

[5] W. Dong, H. Xin, Di Wu, and L. Huang, "Small Signal Stability Analysis of Multi-Infeed Power Electronic Systems Based on Grid Strength Assessment," *IEEE Trans. Power Syst.*, vol. 34, no. 2, 2019.

[6] Y. Zhang, H. Jin, H. Becker, and M. Braun, *Quantifying Oscillatory Mode Damping of Power Systems via Frequency-Domain Analysis*, 2025.

[7] Y. Zhu, T. C. Green, X. Zhou, Y. Li, D. Kong, and Y. Gu, "Impedance Margin Ratio: a New Metric for Small-Signal System Strength," *IEEE Trans. Power Syst.*, 2024.

[8] CIGRE WG B4.62, "Connection of wind farms to weak AC networks," TB671, 2017.

[9] C. Henderson et al., "Grid Strength Impedance Metric: An Alternative to SCR for Evaluating System Strength in Converter Dominated Systems," *IEEE Trans. Power Delivery*, vol. 39, no. 1, 2024.

[10] Y. Lamrani et al., "Frequency-Averaged Grid Impedance Metric for Identifying Weakest Buses in Power Electronics-Dominated Systems," in *2025 IEEE Kiel PowerTech*, Kiel, Germany, Jun. 2025 - Jul. 2025.

[11] Y. Zhou *et al.*, "Small-Signal Stability Assessment of Heterogeneous Grid-Following Converter Power Systems Based on Grid Strength Analysis," *IEEE Trans. Power Syst.*, vol. 38, no. 3, 2023.

[12] Y. Li et al, "Impedance Circuit Model of Grid-Forming Inverter: Visualizing Control Algorithms as Circuit Elements," *IEEE Trans. Power Electron.*, vol. 36, no. 3, 2021.

[13] W. Du *et al.*, "A Comparative Study of Two Widely Used Grid-Forming Droop Controls on Microgrid Small-Signal Stability," *IEEE J. Emerg. Sel. Topics Power Electron.*, vol. 8, no. 2, 2020.

[14] C. Zhang et al., "On the Relation of Nodal Admittance- and Loop Gain-Model Based Frequency-Domain Modal Methods for Converters-Dominated Systems," *IEEE Trans. Power Syst.*, vol. 38, no. 2, 2023.

[15] Y. Zhu, Y. Gu, Y. Li, and T. C. Green, "Impedance-Based Root-Cause Analysis: Comparative Study of Impedance Models and Calculation of Eigenvalue Sensitivity," *IEEE Trans. Power Syst.*, vol. 38, no. 2, 2023.

[16] C. Liu et al., "Generalized Operational Short-Circuit Ratio for Grid Strength Assessment in Power Systems With High Renewable Penetration," *IEEE Trans. Power Syst.*, vol. 39, no. 4, 2024.

979-8-3315-8138-1